JTTEE5 14:335-341
DOI: 10.1361/105996305X59350
1059-9630/$19.00 © ASM International

High-Velocity Oxyfuel Cr_3C_2-NiCr Replacing Hard Chromium Coatings

J.M. Guilemany, N. Espallargas, P.H. Suegama, A.V. Benedetti, and J. Fernández

(Submitted October 18, 2004; in revised form March 11, 2005)

Comparative wear and corrosion properties of Cr_3C_2-NiCr (CC-TS) (a high-velocity oxyfuel [HVOF]) and hard chromium (HC) coatings obtained on a steel substrate have been studied. The structural characterization was done before and after measurements by optical microscopy, scanning electron microscopy, and scanning white light interferometry. Wear and corrosion properties were evaluated by ball on disk (ASTM G99-90), rubber wheel (ASTM G65-91), and electrochemical measurements of open circuit and polarization curves. The best corrosion and wear resistance was for the CC-TS obtained by HVOF. The open-circuit potential values measured for both samples after 18 h of immersion were: −0.240 and −0.550 V, respectively, for CC-TS and HC, versus Ag/AgCl,KCl_{sat}. Three orders of magnitude lower volume loss were found for CC-TS (HVOF) after friction tests compared with HC.

Keywords: corrosion resistance, Cr_3C_2-NiCr, hard chromium, high-velocity oxyfuel, thermal spray, wear

1. Introduction

Conventional hard chromium (HC) plating, which is widely applied in the engineering industry to improve the surface properties of critical components, is produced from chromic acid solutions containing chromium in the hexavalent state and catalytic anions. These coatings, the thicknesses of which are in the range of 20 to 200 μm for external areas and up to 500 μm as a rebuild coating, have as main properties high hardness, corrosion resistance, as well as good wear behavior. Chromium plating properties, such as hardness and microcrack density, change with, for instance, the bath composition, current density, and bath temperature (Ref 1, 2). Conventional HC has a structure that is based in a crack network and a superficial oxidation due to passivation.

Hard chromium coatings are expensive due to the posttreatment needed after deposition, like mechanization and trapped-hydrogen thermal removing. It is well known that chrome plating hardness decreases at temperatures above 350 °C, making it unsuitable to be used for wear resistance in applications in which the working temperature is higher than 450 °C.

In addition, the new European legislation concerned with the hazardous wastes of galvanic industries has promoted the research of alternative processes to chromium plating due to environmental pollution by Cr(VI) compounds known to be carcinogenic (Ref 3, 4).

Over the last few years, thermal spray coatings, such as Cr_3C_2-NiCr (CC-TS) and tungsten carbide coatings, appear to be the best alternative to HC plating in most cases (Ref 3-6). With high-velocity oxyfuel (HVOF) processes, low-porosity metallic and cermet coatings can be achieved, having good oxidation resistance and adherence properties as well as deposition rates that are faster than electroplating (Ref 7-9).

Coatings based on WC have better wear and fatigue properties than HC (Ref 8, 10, 11). Spray powders like WC-Co and WC-CoCr are commonly used as an alternative to HC plating when it is applied, for instance, in aircraft manufacturing (Ref 5). When the application requires improved corrosion resistance, the use of CoCr as a metal matrix is the best alternative. On the other hand, the maximum application temperature of WC-based coatings is in the range of 400 to 450 °C.

When the attributes of tungsten carbide coatings are not suitable to fulfill the requirements of the applications, CC-TS coatings have been extensively used to minimize high-temperature wear and corrosion processes (Ref 12). These coatings have good abrasion and friction resistance up to 850 °C, due to their high thermal stability and good oxidation resistance. Corrosion resistance is provided by the NiCr matrix, while wear resistance is mainly due to its ceramic phase (carbides) (Ref 6). The high chemical stability of CC-TS coatings allows these coatings to be used as alternatives to HC plating in applications where wear and corrosion resistance are required.

The corrosion properties of thermal spray coatings in a corrosive media (e.g., 3.4%NaCl or 0.5%H_2SO_4) have been studied by some authors (Ref 7, 13-15). In most cases, the mechanism of electrolyte penetration through the coating, which affects the electrochemical behavior of a cermet coating, is still under consideration.

The aim of the current study is to compare the corrosion and wear resistance of HC and HVOF thermally sprayed CC-TS. The friction and abrasion resistance of both coatings have been compared.

2. Experimental

An UNS-G41350 steel alloy was used as a substrate. Rectangular (100 × 20 × 5 mm^3) and cylindrical (ø = 25.4 mm, height =

J.M. Guilemany, N. Espallargas, and **J. Fernández,** Thermal Spray Centre, Materials Engineering, Departimento Ingeniería Química y Metalurgia, Universidad de Barcelona, C/Martí i Franquès 1, CP 08028 Barcelona, Spain; and **P.H. Suegama** and **A.V. Benedetti,** Departimento Físico-Química, Instituto de Química, Universidade Estadual Paulista, UNESP, CP 355, 14801-970 Araraquara, SP, Brasil. Contact e-mail: cpt-cmem@ub.edu.

25.4 mm) coupons were degreased with acetone and grit-blasted with Al_2O_3 to get a roughened surface (mean roughness [Ra] ~5 μm).

At the Thermal Spray Center of the University of Barcelona, CC-TS coatings were applied by HVOF using Sulzer Metco (Westbury, NY) Diamond Jet Hybrid DJH 2700 equipment, using propylene as the fuel gas and oxygen to partially melt the powder particles and spray them onto the steel substrate. The powder selected was a commercial 80wt.%Cr_3C_2-20wt.%NiCr.

Samples of CC-TS were obtained by the optimization of the spray parameters. Samples of conventional HC-coated steel were provided by an electroplating industry, using conventional routes (Ref 2).

The thicknesses of all coatings were determined in the transverse section using the MATROX INSPECTOR Image Analysis software (Matrox, Dorval, Canada).

The microstructures of all the coatings were studied using an optical microscope (OM) and a scanning electron microscope (SEM) coupled to an energy-dispersive spectrometer analyzer (EDS).

Friction tests were carried out using ball-on-disk (BOD) equipment according to the ASTM G99-90 standard. A hard metal ball 11 mm in diameter and a hardness of HVN_{300} = 1700 was used as the counterface. The environmental conditions were held constant during the test, the relative humidity and temperature being 20% and 20 °C, respectively. The sliding distance was kept at 1000 m for all tests. A track diameter of 16 mm, a sliding speed of 0.11 m/s, a load of 10 N, and a final coating Ra of 0.2 to 0.4 μm was used (to get this Ra value, it is necessary to polish the samples only for the BOD test). The friction force was recorded during the test. The friction energy was calculated as the area under the friction force versus the accumulated sliding distance. Friction coefficients were calculated from the average value measured in the last 200 m. The wear tracks produced in the coatings were studied using SEM. The damage was evaluated using scanning white light interferometry (SWLI), and the results of coating volume loss are reported.

Abrasion tests were carried out with a rubber wheel test machine according to the ASTM G65-91 standard, using SiO_2 with particles 0.4 to 0.8 mm in size as the abrasive material. The weight lost was used to compare the abrasion resistance and to calculate the abrasive wear rate of the different samples. The duration of the tests was 30 min, and the material lost was measured by weighting the samples every 1 min for 5 min and then every 5 min until the end of the test. To express the wear rate in terms of the material removed, the density of the coatings was used to transform the mass in volume.

Cross-sectional microhardness measurements were performed by means of Vickers indentation at a load of 300 g, and the indentations were measured with an OM to increase measurement accuracy. Values quoted are an average of 20 indentations for each coating.

The structure of the powder and coatings was analyzed using a Siemens D500 diffractometer (Siemens, Munich, Germany) [K_α (Cu) = 1.54, 40 kV, 30 mA] to follow the structural changes that can take place during the spraying.

The corrosion resistance of samples was evaluated by means of electrochemical measurements in 80 mL of an aerated and unstirred 3.4%NaCl solution. An Ag/AgCl, KCl-saturated electrode connected to the solution through a Luggin capillary was used as a reference electrode and a Pt network was the auxiliary electrode. A working electrode of each coated sample was fixed at the bottom of the electrochemical cell, exposing an area of 1 cm^2 to the solution. Open-circuit (E_{OC} versus time) and polarizations curve (C_P) measurements were done using an EG&G Parc-273 (Princeton, NJ). Polarization experiments were carried out in a potential range from –100 to +350 mV versus an E_{OC} at 0.166 mV/s.

The salt fog spray tests were carried out according to the ASTM B117-90 standard, using 5% NaCl solution at 35 °C. Samples were verified each 24 h until the corrosion products were observed on the surface.

3. Results and Discussion

3.1 Structural Characterization

3.1.1 Cr_3C_2-NiCr Powder. The CC-TS powder used was commercially available. It was a clad composite with each carbide phase completely clad with a nickel chromium alloy with a mean particle size of 25 μm (Fig. 1a). The metal cladding mini-

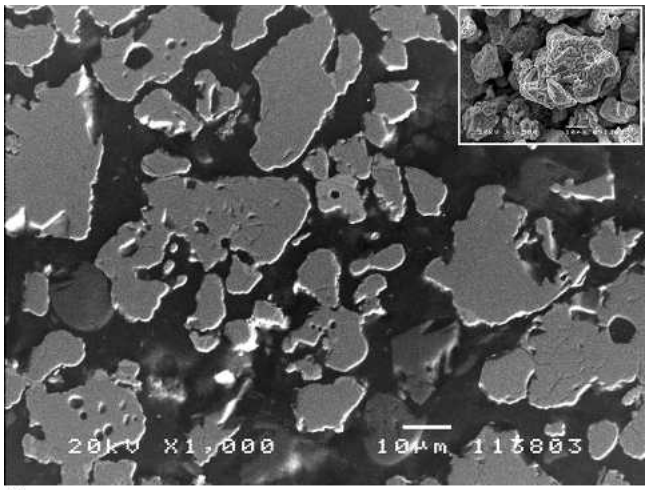

(a)

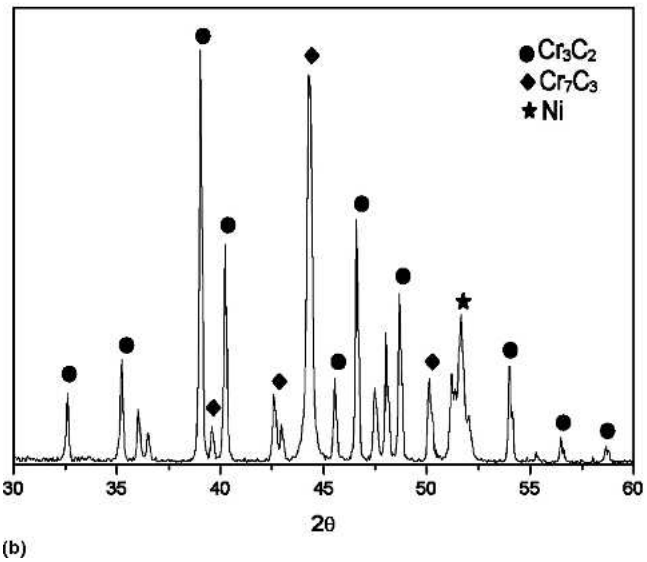

(b)

Fig. 1 CC-TS powder: (a) SEM cross-sectional images (inset: rough surface images), and (b) XRD spectra

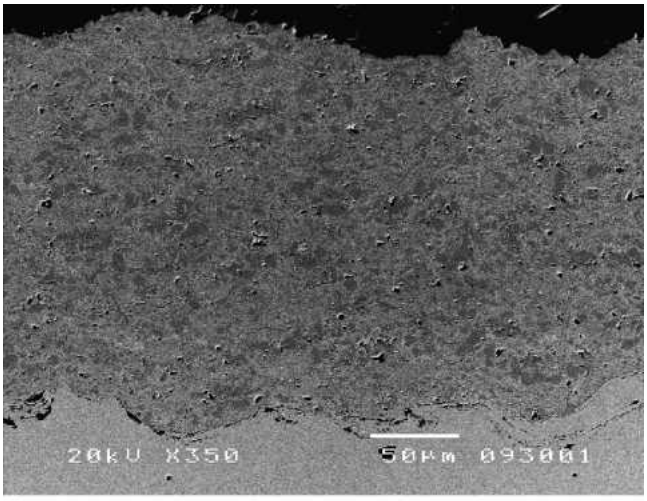

(a)

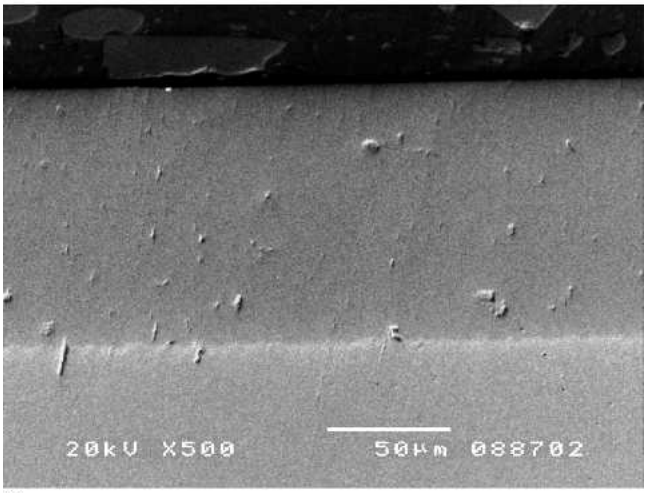

(b)

Fig. 2 SEM cross-sectional image of (a) the CC-TS sample and (b) the HC sample

mizes the decarburization of the chromium carbide phase during the spraying process, providing more efficient deposition.

The x-ray diffraction (XRD) study of powder showed its crystallinity and the phases Cr_3C_2, Cr_7C_3, and NiCr matrix (Fig. 1b).

3.1.2 The Coatings. The structural characterization of the coated samples showed well-bonded layers with thicknesses of 220 and 100 µm and mean microhardness values of 1150 ± 21 HVN_{300} and 1100 ± 28 HVN_{300}, respectively, for samples CC-TS (the HVOF) and HC (electroplated). Figure 2 shows the structures of CC-TS (Fig. 2a) and HC (Fig. 2b). Due to the spraying technique used in the CC-TS coating, melted and semi-melted particles (the particles are a mixture of Cr_3C_2 in a NiCr matrix) were observed, making the coating more heterogeneous than HC coatings. Figure 3 shows the cross-sectional structure of the CC-TS coating, which consists of a nanocrystalline-NiCr matrix (A) with different percentages of chromium (20–50 wt.%), as previously shown (Ref 16), and carbides such as Cr_7C_3 produced by partial decomposition of the initial Cr_3C_2 (B), during the spraying process (Ref 16). Low Cr_2O_3 (C) content was detected; pores (D) and small cracks were seen between the different deposited layers.

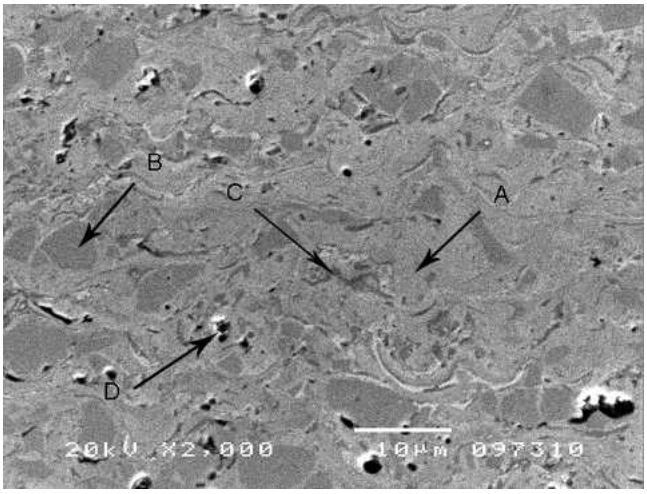

Fig. 3 SEM cross-sectional image of the CC-TS sample

Figure 4 shows a SEM image of the surface of the CC-TS sample (Fig. 4a) and the HC sample (Fig. 4b). Notice that the HC sample shows the typical cracks present in conventional HC deposits, and the CC-TS sample presents splats formed during the spray process.

X-ray diffraction analyses, which were carried out to identify the different phases for both samples, are shown in Fig. 5. The HC sample has a thin oxide film on the surface due to the high tendency of chromium to oxidize. As this layer is too thin, the XRD beam penetrates the chromium oxide film and interacts with the bulk material (metallic chromium). For this reason, the XRD showed only peaks attributed to metallic chromium. The XRD of the CC-TS coatings showed Cr_3C_2, Cr_7C_3, Cr_2O_3, and Ni phases. The Cr_2O_3 phase is formed by Cr oxidation during the spraying process. The CC-TS spectra shows a broader region between $2\theta \approx 35°$ to 50°, indicating an amorphous or nanocrystalline state of the coating. This coating structure could be attributed to both the spray parameters and the powder morphology.

3.2 Friction Test (Ball-on-Disk)

Ball-on-disk tests were carried out to measure the sliding wear resistance. Results showed the best behavior against friction for CC-TS samples. Table 1 lists the main wear properties (i.e., coating volume loss, wear track depth and width, friction coefficient, and energy dissipation) for the samples tested.

For the CC-TS sample, the volume loss is three orders of magnitude lower than that for the HC sample. Small but significant differences in the friction coefficient and dissipated energy can be seen between the coatings, indicating lower values for the CC-TS sample. There is a correlation between the dissipated energy and the coating volume loss; the higher the dissipated energy, the lower the coating wear resistance. Figure 6 shows the differences in the wear tracks and the dimensions of the wear tracks between the samples. Note the substantial differences in

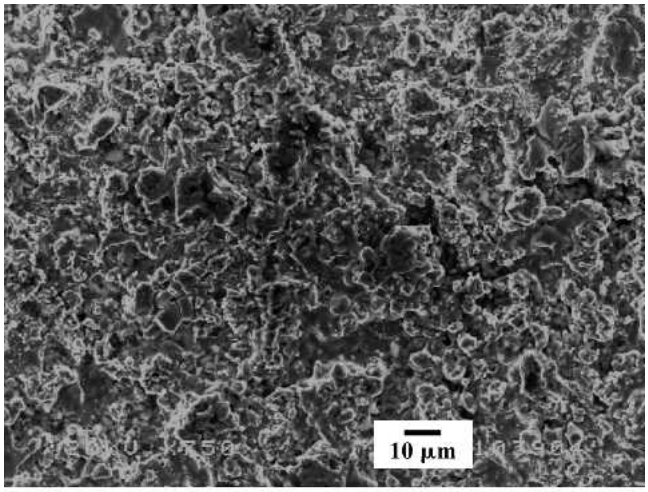

(a)

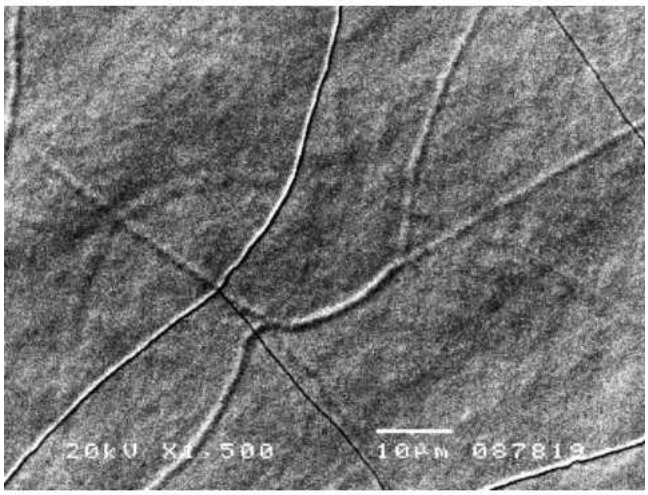

(b)

Fig. 4 SEM surface image of (a) the CC-TS sample and (b) the HC sample

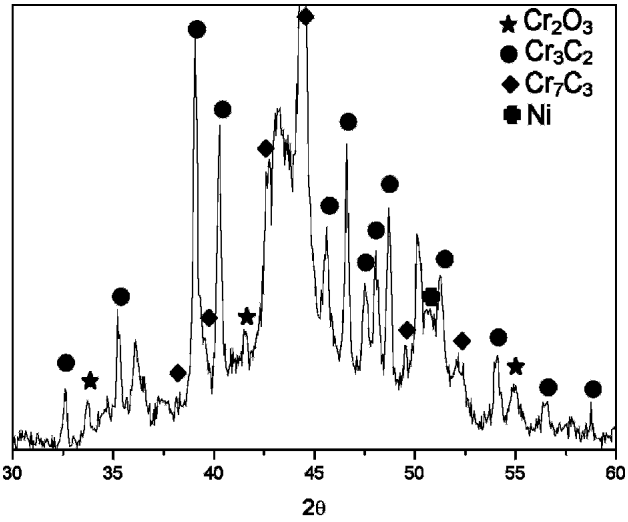

(a)

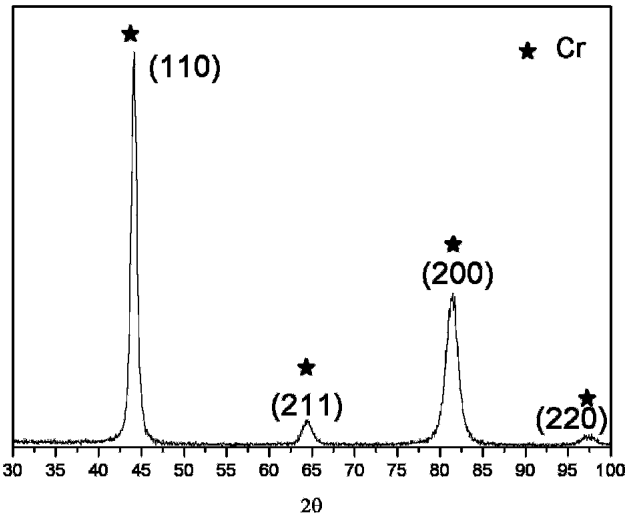

(b)

Fig. 5 XRD spectra of (a) the CC-TS sample and (b) the HC sample

the wear damage between the CC-TS sample (Fig. 6a) and the HC sample (Fig. 6b). After the BOD tests, the width and depth were approximately 5 and 50 times greater, respectively, for the HC sample than for the CC-TS sample, indicating a better performance of the CC-TS coating. Wear parameters are affected by the different natures of the coatings (the CC-TS sample is a coating consisting of agglomerated ceramic particles in a metallic matrix, while the HC sample consists of a metallic and uniform coating), showing that wear parameters are strongly affected by the structure and composition of the coatings.

A SEM study of the wear tracks was performed for both samples. In both cases, wear tracks have debris (Fig. 7) as a result of the pull out of the coating material and its counterface. The contact between the coating and the counterface at the beginning of the test results in an abrasive wear mechanism due to the higher ball hardness. After a certain number of cycles, the adhesive wear mechanism appears when the Ra of the coating decreases due to the sliding. The volume loss of the HC coatings increases due to its crack network structure. The presence of debris on the wear track made the sliding easier in the CC-TS samples than in the HC samples, which resulted in less wear. For the CC-TS sample, the debris seems to be more adhered to the surface, acting as a lubricant, while for the HC sample the debris is less attached to the coating and then is pulled out during the friction test, increasing the amount of material that is lost.

Table 1 Main wear properties(a)

Properties	CC − TS	HC
Volume loss, mm^3	$6.9 \times 10^{-3} \pm 1.56 \times 10^{-4}$	2.5 ± 0.05
Width, mm	0.382 ± 0.06	1.780 ± 0.09
Depth, µm	0.90 ± 0.05	59.94 ± 0.06
Friction coefficient, µ	0.498 ± 0.02	0.557 ± 0.07
Energy, kJ	5.11 ± 0.04	5.50 ± 0.07

(a) Values given as mean ± SD

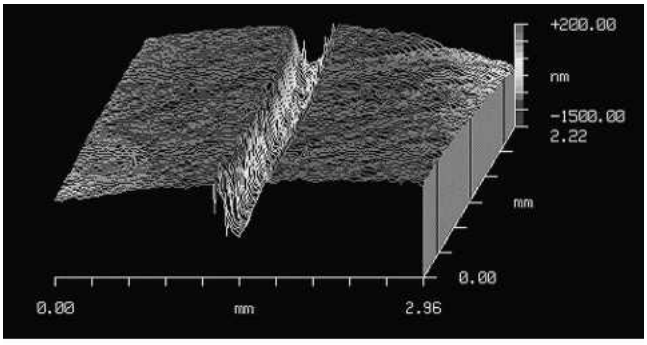

(a)

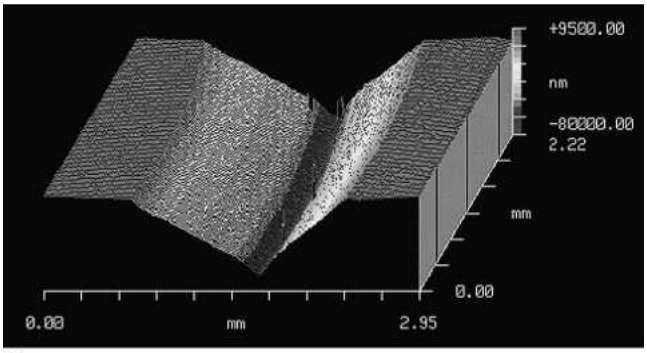

(b)

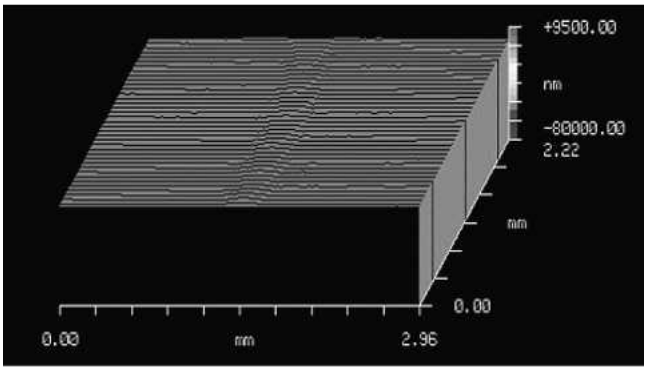

(c)

Fig. 6 SWLI images of the wear tracks of (a, c) the CC-TS sample and (b) the HC sample. The scale of the *z*-axis in (b) and (c) is the same. Note the substantial differences in the wear damage between (c) the CC-TS sample and (b) the HC sample.

3.3 Abrasive Wear Tests (Rubber Wheel)

Abrasion tests are commonly carried out without a before test ground of the samples. All samples are tested with the initial Ra, which is 3 μm for the CC-TS as-sprayed sample and 0.5 μm for the HC sample. Abrasion tests showed that the CC-TS coating has higher weight losses than the HC coating. The weight lost from the CC-TS sample was 0.023 g versus 0.007 g for the HC sample, which means that the CC-TS coating suffers higher abrasion wear than the HC coating. Figure 8 shows the abrasive wear rate versus time during testing. For shorter testing times, the decrease in the wear rate is higher in the CC-TS sample than in the HC sample due to the different initial surface Ra. This

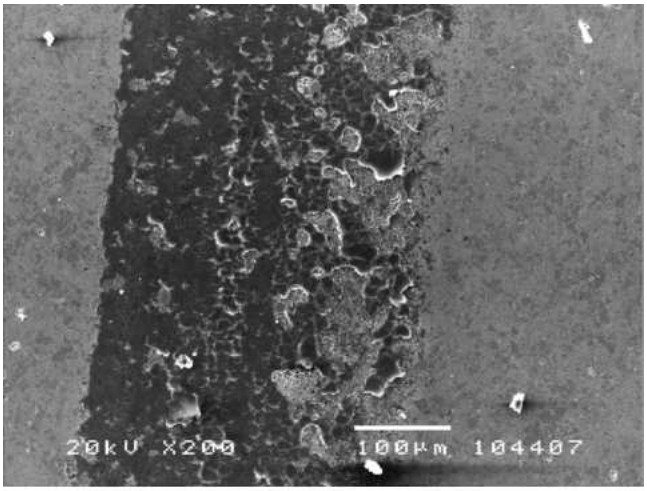

(a)

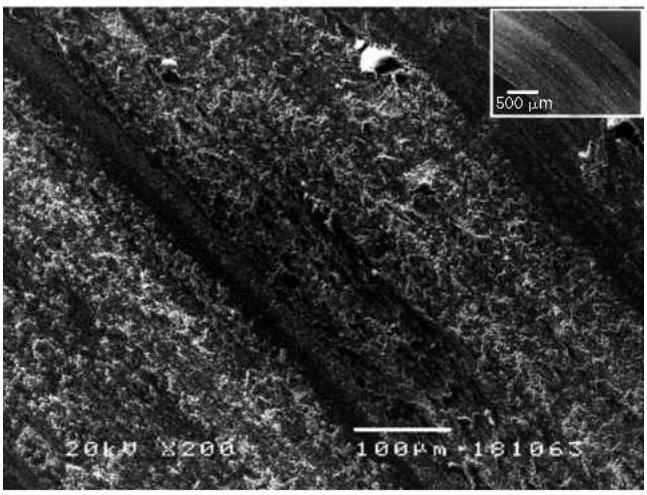

(b)

Fig. 7 Wear tracks on the as-sprayed coatings: (a) CC-TS sample, and (b) HC sample

difference decreases until a steady state is achieved, then the wear rate of the sample begins to stabilize.

The wear rates were 5.79×10^{-6} and 2.48×10^{-5} mm^3 · N/m, respectively, for the HC and CC-TS samples. These results are in agreement with the different natures of the coatings, which influenced their behavior in the abrasion tests. The CC-TS coating is much more brittle than the HC coating because the CC-TS coating has 80% of a ceramic phase. This fact shows that toughness plays an important role in the way abrasion is taking place. Compared with the CC-TS coating, the higher degree of toughness of the HC coating explains the higher abrasion resistance.

3.4 Corrosion Measurements

3.4.1 Open-Circuit Measurements and Polarization Plots. Figure 9 shows the open-circuit potential curves for samples of the CC-TS coating, the HC coating, and the steel substrate. Potential decay was observed, which was due to the dissolution of surface oxides, chloride adsorption, and the pen-

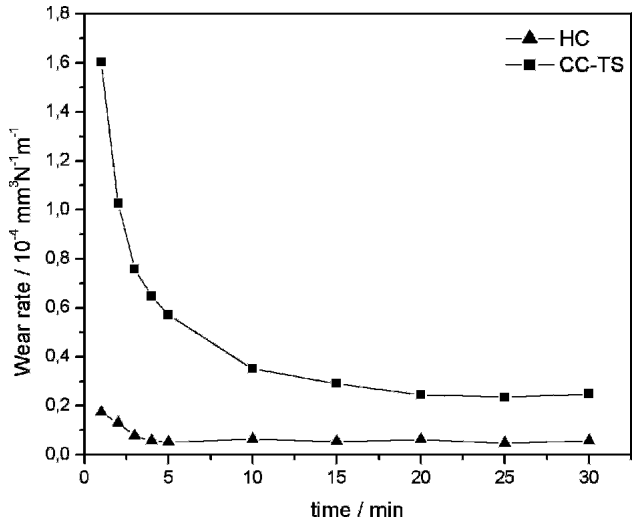

Fig. 8 Wear rate of the CC-TS and HC samples versus time

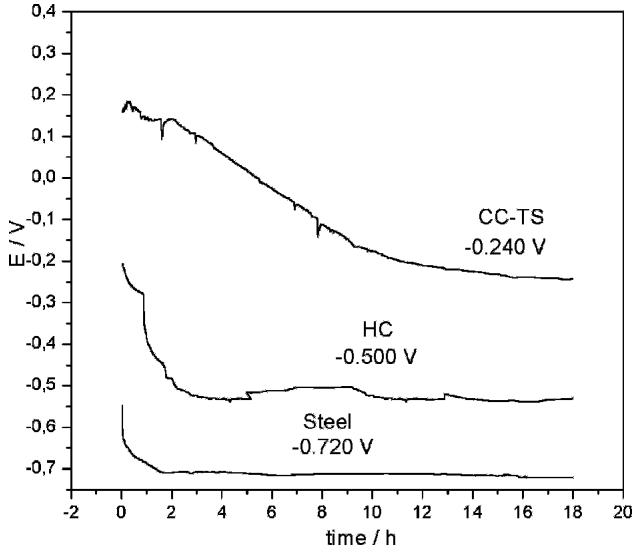

Fig. 9 Open-circuit potential (E_{OC}) versus time curves for different coatings and the substrate, obtained in an aerated and unstirred 3.4% NaCl solution at 25 °C

etration of electrolytes into the coating. After ~1.5 h of immersion, the HC coating shows more potential decay stabilizing at a potential lower than the initial potential and closer to the substrate potential (i.e., −0.72 V), which indicates that the electrolyte reached the steel substrate. On the other hand, the CC-TS coating presents a lower decay potential and stabilizes at a higher potential than the HC coating. For the CC-TS sample, the electrolyte did not reach the steel substrate even after 130 h of immersion, because no corrosion products were detected on the cross-sectional EDS analysis.

The polarization curves, which were recorded after the open-circuit potential tests, for the CC-TS coating, the HC coating, and the steel substrate samples that were obtained in a 3.4% NaCl solution are shown in Fig. 10. The CC-TS sample presented a more positive E_{corr} (potential in the steady state, after

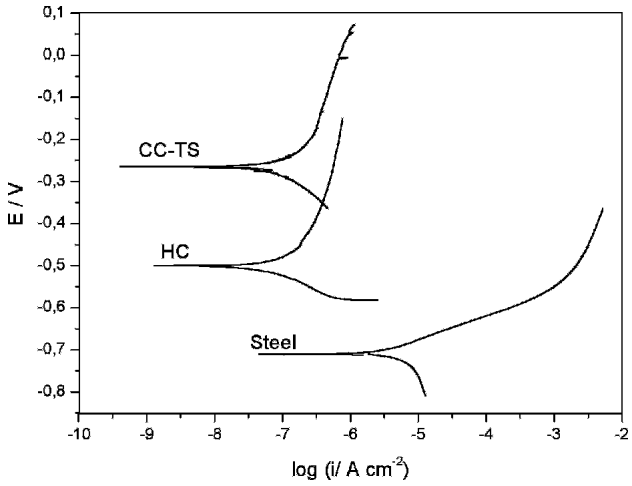

Fig. 10 Polarization curves for coated steels and the substrate in an aerated and unstirred 3.4% NaCl solution at 25 °C and v = 0.166 mV/s

18 h of immersion) and a lower current intensity than the HC sample, indicating that the CC-TS sample has higher corrosion resistance in this environment.

3.4.2 Salt Fog Spray Test. In the salt fog spray test, the CC-TS coating was subjected to a total exposure of 1000 h, and no corrosion products were observed on the surface. The HC coating showed corrosion products on the surface after 500 h of exposure. Using EDS, these corrosion products, which originated from the substrate, were identified as iron oxides only in the HC samples.

4. Conclusions

Thermal spray coating showed better friction wear behavior (BOD) than HC, resulting in three orders of magnitude lower volume of material lost for the thermally sprayed sample. An HC coating has a lower sliding resistance, increasing the volume of material lost due to the crack network structure.

The HC coating showed a better abrasion wear rate, but by only one order of magnitude. Toughness plays an important role in the three-body abrasion process, showing that it is necessary to optimize the thermal spray parameters to improve abrasive wear.

The salt fog and electrochemical tests showed better resistance for the thermal spray coating. For the salt fog tests, corrosion products were not found on the thermally sprayed surface, even after 1000 h of testing. The sample, which was thermally sprayed using HVOF, showed a higher corrosion potential than the HC coating, and the electrolyte did not reach the steel substrate even after 130 h in a 3.4% NaCl solution.

The thermal spray coating had great friction wear behavior and a high corrosion resistance in the NaCl solution, and can be an alternative to an HC coating.

Acknowledgments

This study was supported by the Universidad de Barcelona by a research grant for Investigación y Docencia to N. Espallar-

gas, the Ministerio de Ciencia y Tecnología (project No. MAT2003-05004-C02-02), the Generalitat de Catalunya (project No. 2001SGR00145), and the Fundação de Amparo à Pesquisa do Estado de São Paulo (No. 02/00448-7).

References

1. L. Fedrizzi, S. Rossi, F. Bellei, and F. Deflorian, Wear Corrosion Mechanism of Hard-Chromium Coatings, *Wear,* Vol 253, 2002, p 1173-1181
2. J.K. Dennis and T.E. Such, *Nickel and Chromium Plating,* Woodhead Publishing Ltd., 3rd ed., 1993
3. U. Erning and M. Nestler, HVOF Coatings for Hard-Chrome Replacement Properties and Applications, *Tagungsband Conference Proceedings,* E. Lugscheider and R.A. Kammer, Ed., March 17-19, 1999 (Düsseldorf, Germany), DVS Deutscher Verband für Schweiβen, p 462-466
4. T. Sahraoui, S. Guessasma, N.E. Fenineche, G. Montavon, and C. Coddet, Friction and Wear Behaviour of HVOF Coatings and Electroplated Hard Chromium Using Neural Computation, *Mater. Lett.,* Vol 58, 2004, p 654-660
5. A.C. Savarimuthu, I. Megat, H.F. Taber, J.R. Shadley, E.F. Rybicki, W.A. Emery, J.D. Nuse, and D.A. Somerville, Sliding Wear Behaviour as a Criterion for Replacement of Chromium Electroplate by Tungsten Carbide (WC) Thermal Spray Coatings in Aircraft Applications, *Thermal Spray: Surface Engineering via Applied Research,* C.C. Berndt, Ed., May 8-11, 2000 (Montréal, Québec, Canada), ASM International, p 1095-1104
6. P.L. Ko and M.F. Robertson, Wear Characteristics of Electrolytic Hard Chrome and Thermal Sprayed WC-10Co-4Cr Coatings Sliding against Al-Ni-Bronze in Air at 21 °C and at −40 °C, *Wear,* Vol 252, 2002, p 880-893
7. P.H. Suegama, C.S. Fugivara, A.V. Benedetti, J. Fernández, J. Delgado, and J.M. Guilemany, Electrochemical Behaviour of Thermally Sprayed Cr_3C_2-NiCr Coatings in 0.5M H_2SO_4 Media, *J. Appl. Electrochem.,* Vol 32, 2002, p 1287-1295
8. J.M. Miguel, "Caracterización Estructural y de Propiedades Tribológicas y Mecánicas de Recubrimientos de Interés Tecnológico Obtenidos por Proyección Térmica," Ph.D. dissertation, Universidad de Barcelona, 2002
9. V. Sobolev, J.M. Guilemany, and J. Nutting, *High Velocity Oxy-Fuel Spraying,* Maney, 2004
10. T. Sahroui, N.E. Fenineche, G. Montavon, and C. Coddet, Wear Behaviour of HVOF Sprayed WC-12%Co Coatings vs. Hard Chrome Plating, *Thermal Spray 2004: Advances in Technology and Application,* ASM International, May 10-12, 2004 (Osaka, Japan), ASM International, 2004
11. V.A. de Souza and A. Neville, Corrosion and Erosion Damage Mechanism during Erosion-Corrosion of WC-Co-Cr Cermet Coatings, *Wear,* Vol 255, 2003, p 146-156
12. S. Matthews, M. Hyland, and B. James, Microhardness Variation in Relation to Carbide Development in Heat Treated Cr_3C_2-NiCr Thermal Spray Coatings, *Acta Mater.,* Vol 51, 2003, p 4267-4277
13. J.M. Guilemany, J. Fernández, A.V. Benedetti, and J. Delgado, Drawbacks in Corrosion Resistance of Thermal Spray Coatings against Aqueous Aggressive Media, *International Thermal Spray Conference,* E. Lugscheider and C.C. Berndt, Ed., March 4-6, 2002 (Essen, Germany), DVS Deutscher Verband für Schweiβen, 2002, p 894-899
14. L. Fedrizzi, S. Rossi, R. Cristel, and P.L. Bonora, Corrosion and Wear Behaviour of HVOF Cermet Coatings Used to Replace Hard Chromium, *Electrochim. Acta,* Vol 49, 2004, p 2803-2814
15. D. Toma, W. Brandl, and G. Marginean, Wear and Corrosion Behaviour of Thermally Sprayed Cermet Coatings, *Surf. Coat. Technol.,* Vol 138, 2001, p 149-158
16. J.M. Guilemany, J.A. Calero, and V. Sobolev, "Effect of the Physical Characteristics and Properties of Powder Particles on the Structural and Mechanical Characterization of Cr_3C_2-NiC Coatings," presented at the 1998 Powder Metallurgy World Congress, Granada, Spain. October, Vol 4, p. 6
17. ASTM Standard G65-91D: Standard Test Method for Wear Measuring Abrasion Using the Dry Sand/Rubber Wheel Apparatus.